

# Uniformly Accurate Machine Learning Based Hydrodynamic Models for Kinetic Equations

JIEQUN HAN<sup>1,\*</sup>, CHAO MA<sup>2</sup>, ZHENG MA<sup>3</sup>, AND WEINAN E<sup>1,2,4</sup>

ABSTRACT. A new framework is introduced for constructing interpretable and truly reliable reduced models for multi-scale problems in situations without scale separation. Hydrodynamic approximation to the kinetic equation is used as an example to illustrate the main steps and issues involved. To this end, a set of generalized moments are constructed first through an autoencoder to optimally represent the underlying velocity distribution. The well-known closure problem is then solved with the aim of best capturing the associated dynamics of the kinetic equation. The issue of physical constraints such as Galilean invariance is addressed and an active learning procedure is introduced to help ensure that the data set used is representative enough. The reduced system takes the form of the conventional moment systems and works regardless of the numerical discretization used. Numerical results are presented for the BGK model. We demonstrate that the reduced model achieves a uniform accuracy in a wide range of Knudsen numbers spanning from the hydrodynamic limit to free molecular flow.

This paper is written with two objectives in mind. The first is about multi-scale modeling. Here our interest is to develop macro-scale models in situations without scale separation. The second is about machine learning. Here our interest is to build interpretable and truly reliable physical models with the help of machine learning. Both objectives are of paramount importance for scientific modeling, and certainly we will not be able to address them completely within one paper. Instead we will restrict ourselves to an illustration of what we consider to be the main issues that are involved, using a relatively simple example: machine learning-based moment closure for kinetic equations.

In scientific modeling, we often encounter the following dilemma: We are interested in modeling some macro-scale phenomenon but we only have a reliable model at some micro scale and the micro-scale model is too detailed and too expensive for practical

---

<sup>1</sup>Department of Mathematics, Princeton University

<sup>2</sup>Program in Applied and Computational Mathematics, Princeton University

<sup>3</sup>Department of Mathematics, Purdue University

<sup>4</sup>Beijing Institute of Big Data Research

\*To whom correspondence should be addressed. E-mail: jiequnh@princeton.edu.

use. The idea of multi-scale modeling is to develop models or algorithms that can efficiently capture the macro-scale behavior of the system, starting from the micro-scale model (see [1, 2] for a review). An example is the modeling of turbulent flows. Here the micro-scale model is the Navier-Stokes equation. This is widely believed to be sufficiently accurate but is too expensive for modeling large scale turbulent flows such as the ones that we face in weather forecasting. The macro-scale model is either a large eddy simulation (LES) model or the Reynolds averaged Navier-Stokes (RANS) equation [3]. These are much less costly but finding truly reliable LES or RANS models has always been a difficult problem. One reason for this difficulty comes from the fact that there is no scale separation that one can make use of. This situation is quite representative in multi-scale modeling: In the absence of scale separation we lack tools that can be used for discovering the relevant variables and finding accurate approximations for the dynamics of these relevant variables.

Machine learning, the second topic that we are concerned with here, is equally broad and important. We are particularly interested in developing physical models using machine learning. There are significant differences between this and traditional machine learning tasks such as the ones in computer vision and data analytics. One is that in the current setting, instead of being given the data, the data is generated using the micro-scale model. The good news is that in principle we can generate an unlimited amount of data. The bad news is that often times the process of generating data is expensive. Therefore it is an important issue to find a data set that is as small as possible and yet representative enough. The second aspect is that we have to be concerned with physical constraints such as symmetry, invariance, and the laws of nature. We have to make a choice between enforcing these constraints explicitly, or enforcing them approximately as a byproduct of accurately modeling the underlying physical process. The third is the interpretability issue. Machine learning models are often black-box in nature. But as a physical model that we can rely on, just as the Schrödinger equation in quantum mechanics or Navier-Stokes equation in fluid mechanics, it cannot just be a black-box completely. Some of these issues have been studied in [4, 5, 6] in the context of modeling inter-atomic force fields.

This paper examines the aforementioned issues systematically in the context of developing new dynamical models. As a concrete example, we will study the problem where the micro-scale model is the kinetic equation, and the macro-scale model is the hydrodynamic model. Besides being a very representative problem in multi-scale modeling, this example is also of great practical interest in its own right. Kinetic equations have found applications in modeling rarefied gases, plasmas, micro-flow, semiconductor devices, complex fluids, and so on. From a computational point of view, kinetic equations are costly to solve due to the dimensionality of the problem

and the multi-dimensional nonlinear integral in the collision term. As a result, there has been a long history of interest in reducing the kinetic model to a hydrodynamic model, going back at least to the work of Grad [7]. Our work is in the same spirit.

A crucial dimensionless number that influences the behavior of the solutions of the kinetic equations is the Knudsen number, defined as the ratio between the mean free path of a particle and typical macroscopic length scale of interest. When the Knudsen number is small, the velocity distribution stays close to local Maxwellians. This is the so-called hydrodynamic regime. In this regime, it is possible to derive hydrodynamic models for some selected macroscopic fluid variables (typically the mass density, momentum, and energy) such as the Euler equations or Navier-Stokes-Fourier equations [8, 9]. These hydrodynamic models are not only much less costly to solve, but also much easier to use to explain experimental observations. They are often in the form of conservation laws with conserved quantities and fluxes. However, when the Knudsen number is no longer small, the hydrodynamic models break down. Direct simulation Monte Carlo (DSMC) method [10, 11, 12] becomes a more preferred choice. DSMC works well in the collision-less limit when the Knudsen number is large, but its computational cost becomes prohibitive when approaching the hydrodynamic regime due to the high collision rate. The significant difference between these two types of approaches creates a problem when modeling transitional flows in which the Knudsen number varies drastically.

Significant effort has been devoted to developing generalized hydrodynamic models as a replacement of the kinetic equation in different regimes, with limited success. These generalized models can be put into two categories. The first are direct extensions of the Navier-Stokes-Fourier equations. One example is the Burnett equation [13]. In these models, no new variables are introduced, but new derivative terms are added. The second are the moment equations. In this case additional moments are introduced and their dynamic equations are derived through the process of “moment closure” using the kinetic equation. The most well-known example is Grad’s 13-moment equations. Much effort has gone into making sure that such moment equations are mathematically well-posed and respect the most important physical constraints, see [9, 14, 15]. However, in both approaches, one has to introduce some uncontrolled truncation in order to obtain a closed system of partial differential equations (PDE).

To develop machine learning-based models, one can also proceed along these two separate directions. One can stay with the original set of hydrodynamic variables (density, momentum and energy), but introduce corrections to the fluxes as functionals of the local (in space) instantaneous hydrodynamic variables. This approach is

relatively straightforward to implement, and it does give reasonably satisfactory results. But in a way it is more like a numerical algorithm than a new reliable physical model. In addition, some of the issues that we mentioned above, which are important for more general multi-scale modeling problems, do not arise. This means that it has a limited value for an illustrative example. For these reasons, the majority of our efforts is devoted to the second category of methods: the moment equations. We explore the possibility of learning new generalized moments, not necessarily polynomials, to better represent the velocity distribution function. We also explore the possibility of learning accurately the dynamical models, instead of resorting to ad hoc closure assumptions. In addition, we develop an active learning procedure in order to ensure that the data sets used to generate these models are representative enough.

Below we use the Boltzmann equation to explain the technical details of our approach. The algorithms are implemented for the BGK (Bhatnagar, Gross and Krook) model [16]. We work with a wide range of Knudsen numbers ranging from  $10^{-3}$  to 10 and different initial conditions. It is easy to see that the methodology developed here is applicable to a much wider range of models, some of which are under current investigation.

There are some recent work on applying machine learning, especially deep learning to study dynamical systems, including representing the physical quantities described by PDEs with physics-informed neural networks [17, 18], uncovering the underlying hidden PDE models with convolution kernels [19, 20] or sparse identification of nonlinear dynamical systems (SINDy) method [21, 22], predicting reduced dynamics with memory effects using long short-term memory (LSTM) recurrent neural networks [23, 24], calibrating the Reynolds stress in the RANS equation [25, 26], and so on. Machine learning techniques have also been leveraged to find proper coordinates for dynamical systems in the spirit of dimensionality reduction [27, 28, 29, 30]. Despite the widespread interests in machine learning dynamical systems, the examples presented in the literature are mainly ODE models or PDE models in which the ground truth is known. This paper stands in contrast to previous works with the aim of learning, from the original micro-scale model, new reduced PDE at the macro scale accurately.

## 1. PRELIMINARIES

Let  $f = f(\mathbf{x}, \mathbf{v}, t): \mathbb{R}^D \times \mathbb{R}^D \times \mathbb{R} \rightarrow \mathbb{R}$  be the one-particle phase space probability density. Consider the following Boltzmann equation in the absence of external forces

$$\partial_t f + \mathbf{v} \cdot \nabla_{\mathbf{x}} f = \frac{1}{\varepsilon} Q(f), \quad (1)$$

where  $\varepsilon$  is the Knudsen number and  $Q$  is the collision operator.  $Q$  satisfies the conditions

$$\int_{\mathbb{R}^D} Q(f)\phi(\mathbf{v}) \, d\mathbf{v} = 0, \quad \phi(\mathbf{v}) = (1, \mathbf{v}, |\mathbf{v}|^2/2)^T. \quad (2)$$

These ensure that density, momentum and energy are conserved during the evolution.

A very important class of distribution functions are the local Maxwellian distribution function

$$f_M(\mathbf{v}) = \frac{\rho}{(2\pi T)^{\frac{D}{2}}} \exp\left(-\frac{|\mathbf{v} - \mathbf{u}|^2}{2T}\right), \quad (3)$$

where  $\rho$ ,  $\mathbf{u}$  and  $T$  are the density, bulk velocity and temperature fields. They are related to the moments of  $f$  through

$$\rho = \int_{\mathbb{R}^D} f \, d\mathbf{v}, \quad \mathbf{u} = \frac{1}{\rho} \int_{\mathbb{R}^D} f\mathbf{v} \, d\mathbf{v}, \quad T = \frac{1}{D\rho} \int_{\mathbb{R}^D} f|\mathbf{v} - \mathbf{u}|^2 \, d\mathbf{v}. \quad (4)$$

In above the dependence on the location and time has been dropped for clarity of the notation. It can be shown that when  $\varepsilon \ll 1$ ,  $f$  stays close to the local Maxwellian distributions [31, 32, 33, 34, 35]. Taking the moments  $\langle \cdot, \phi \rangle := \int \cdot \phi(\mathbf{v}) \, d\mathbf{v}$  on both sides of the Boltzmann equation (1) with  $\phi$  in (2) and replacing  $f$  by  $f_M$ , one obtains the compressible Euler equations:

$$\begin{cases} \partial_t \rho + \nabla_{\mathbf{x}} \cdot (\rho \mathbf{u}) = 0, \\ \partial_t (\rho \mathbf{u}) + \nabla_{\mathbf{x}} \cdot (\rho \mathbf{u} \otimes \mathbf{u} + p \mathbf{I}) = 0, \\ \partial_t E + \nabla_{\mathbf{x}} \cdot ((E + p)\mathbf{u}) = 0, \end{cases} \quad (5)$$

where  $p = \rho T$  is the pressure and  $E = \frac{1}{2}\rho|\mathbf{u}|^2 + \frac{D}{2}\rho T$  is the total energy. Let

$$\mathbf{U} = \begin{pmatrix} \rho \\ \rho \mathbf{u} \\ E \end{pmatrix}, \quad \mathbf{F}_{\text{Euler}}(\mathbf{U}) = \begin{pmatrix} \rho \mathbf{u}^T \\ \rho \mathbf{u} \otimes \mathbf{u} + p \mathbf{I} \\ (E + p)\mathbf{u}^T \end{pmatrix}, \quad (6)$$

we can rewrite the Euler equations in a succinct conservation form

$$\partial_t \mathbf{U} + \nabla_{\mathbf{x}} \cdot \mathbf{F}_{\text{Euler}}(\mathbf{U}) = 0. \quad (7)$$

For larger values of  $\varepsilon$  one would like to use the moment method to obtain similar systems of PDEs that serve as an approximation to the Boltzmann equation. To this end, one starts with a linear space  $\mathbb{M}$  of functions of  $\mathbf{v}$  (usually chosen to be polynomials) that include the components of  $\phi$  in (2). Denote by  $\mathbf{m}$ , a vector whose components form a basis of  $\mathbb{M}$ . Then the moments  $\mathbf{M}$ , as functions of  $\mathbf{x}$  and  $t$ , are

defined as  $\int_{\mathbb{R}^D} f \mathbf{m}(\mathbf{v}) d\mathbf{v}$ . From the Boltzmann equation, one obtains

$$\partial_t \mathbf{M} + \nabla_{\mathbf{x}} \cdot \int_{\mathbb{R}^D} f \mathbf{m}(\mathbf{v}) \mathbf{v}^T d\mathbf{v} = \int_{\mathbb{R}^D} \frac{1}{\varepsilon} Q(f) \mathbf{m}(\mathbf{v}) d\mathbf{v}. \quad (8)$$

The challenge is to approximate the two integral terms in (8) as functions of  $\mathbf{M}$  in order to obtain a closed system. This is the well-known ‘‘moment closure problem’’ and it is at this stage that various uncontrolled approximations are introduced. In any case, once this is done one obtains a closed system of the form

$$\begin{cases} \partial_t \mathbf{U} + \nabla_{\mathbf{x}} \cdot \mathbf{F}(\mathbf{U}, \mathbf{W}) = 0, \\ \partial_t \mathbf{W} + \nabla_{\mathbf{x}} \cdot \mathbf{G}(\mathbf{U}, \mathbf{W}) = \frac{1}{\varepsilon} \mathbf{R}(\mathbf{U}, \mathbf{W}). \end{cases} \quad (9)$$

Here the moments  $\mathbf{M}$  are decomposed as  $\mathbf{M} = (\mathbf{U}, \mathbf{W})$ , where  $\mathbf{U} \in \mathbb{R}^{D+2}$  denotes the conserved quantities including mass density, momentum and energy, and  $\mathbf{W} \in \mathbb{R}^M$  are the extra new moments. Note that the term  $1/\varepsilon$  is inherited directly from the Boltzmann equation (1).

## 2. MACHINE LEARNING-BASED MOMENT SYSTEM

We are interested in approximating a family of kinetic problems, in which the Knudsen number may span from the rarefied gas regime to the hydrodynamic limit, and the initial conditions are sampled from a wide distribution of profiles. Fig. 1 presents a schematic diagram of the framework for the machine learning-based moment method. Below we first describe the method for learning generalized moments and addressing the moment closure problem. Then we discuss how to build the data set  $\mathcal{D}$  incrementally to achieve efficient data exploration.

**2.1. Learning Generalized Moments.** For this discussion, we can neglect the dependence of  $f$  on  $(\mathbf{x}, t)$  and view  $f$  as a function of the velocity  $\mathbf{v}$  only. When  $f$  is at the local equilibrium, the distribution of velocity can be perfectly described by the macroscopic variables  $\mathbf{U}$  through (3). In other words, the space of velocity densities  $f(\cdot)$  is reduced to a finite,  $(D + 2)$ -dimensional space without any loss of information under the Maxwellian assumption. This can be interpreted as a special autoencoder [36, 37]. Up to the bijection between the conserved quantities  $\mathbf{U}$  and non-conserved quantities  $(\rho, \mathbf{u}, T)$ , the encoder  $\Psi$  maps  $f(\cdot)$  to the moments  $\mathbf{U}$  through (4) and the decoder  $\Phi$  maps  $\mathbf{U}$  back to  $f$  through (3).

When  $f$  is no longer at the local equilibrium, the accuracy for the procedure described above breaks down. Still one can try to find an optimal set of generalized moments that minimize the discrepancy. More concretely, we wish to find a new

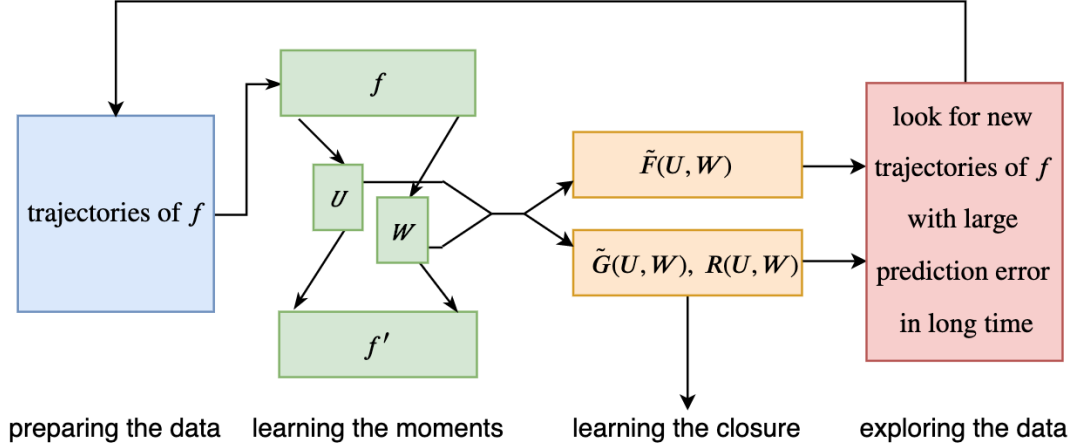


FIGURE 1. Schematic diagram of the machine learning-based moment method

encoder  $\Psi$  that maps  $f$  to generalized moments  $\mathbf{W} \in \mathbb{R}^M$  and a decoder  $\Phi$  that recovers the original  $f$  from  $(\mathbf{U}, \mathbf{W})$ :

$$\mathbf{W} = \Psi(f) = \int_{\mathbb{R}^D} f(\mathbf{v}) \mathbf{w}(\mathbf{v}) d\mathbf{v}, \quad \Phi(\mathbf{U}, \mathbf{W})(\mathbf{v}) = \exp(h(\mathbf{v}; \mathbf{U}, \mathbf{W})). \quad (10)$$

The exponential form is chosen in order to ensure positivity of the reconstructed density. As an auxiliary goal, we would also like to predict a macroscopic analog of the entropy  $\eta$

$$\eta(f) = \int_{\mathbb{R}^D} -f \ln f d\mathbf{v},$$

with all the available moments. Accordingly, the objective function to be minimized reads

$$\mathbb{E}_{f \sim \mathcal{D}} [\|f - \Phi(\mathbf{U}, \Psi(f))\|^2 + \lambda_\eta (\eta(f) - h_\eta(\mathbf{U}, \Psi(f)))^2]. \quad (11)$$

The hypothesis space for  $\mathbf{w}, h, h_\eta$  can be any machine learning models. In this work we choose them to be multilayer feedforward neural networks. In practice the  $f$ 's are always discretized into finite dimensional vectors and the quantities in (11) are actually squared  $l^2$  norms of the associated vectors. Once the optimal functions  $\mathbf{w}, h, h_\eta$  are trained,  $\mathbf{W} = \Psi(f)$  provides the generalized moments of the system.

**2.2. Learning Moment Closure.** Recall the dynamic equation (9) for the moment system, the goal of moment closure is to find suitable approximations of  $\mathbf{F}, \mathbf{G}, \mathbf{R}$  as

functions of  $(\mathbf{U}, \mathbf{W})$ , without any dependence of  $\varepsilon$ . We first rewrite (9) into

$$\begin{cases} \partial_t \mathbf{U} + \nabla_{\mathbf{x}} \cdot [\mathbf{F}_0(\mathbf{U}) + \tilde{\mathbf{F}}(\mathbf{U}, \mathbf{W})] = 0, \\ \partial_t \mathbf{W} + \nabla_{\mathbf{x}} \cdot [\mathbf{G}_0(\mathbf{U}) + \tilde{\mathbf{G}}(\mathbf{U}, \mathbf{W})] = \frac{1}{\varepsilon} \mathbf{R}(\mathbf{U}, \mathbf{W}), \end{cases} \quad (12)$$

where  $\mathbf{F}_0(\mathbf{U}), \mathbf{G}_0(\mathbf{U})$  are the fluxes of the corresponding moments  $\mathbf{U}, \mathbf{W}$  under the local Maxwellian distribution, that is,  $\mathbf{F}_0(\mathbf{U}) \equiv \mathbf{F}_{\text{Euler}}(\mathbf{U})$  and

$$\mathbf{G}_0(\mathbf{U}) = \int_{\mathbb{R}^D} f_M(\mathbf{v}; \mathbf{U}) \mathbf{w}(\mathbf{v}) \mathbf{v}^T d\mathbf{v}.$$

Here we denote by  $f_M(\cdot; \mathbf{U})$  the Maxwellian distribution defined by the macroscopic variables  $\mathbf{U}$ . Our experience has been that separating the terms  $\mathbf{F}_0(\mathbf{U})$  and  $\mathbf{G}_0(\mathbf{U})$  out from  $\mathbf{F}$  and  $\mathbf{G}$  serves to reduce the variance during training. In practice, we can calculate  $\mathbf{w}(\cdot)$  on a few points in advance and use the Gauss-Legendre quadrature rule to approximate  $\mathbf{G}_0(\mathbf{U})$  efficiently. Now our goal becomes finding  $\tilde{\mathbf{F}}, \tilde{\mathbf{G}}, \mathbf{R}$ . Note that the only non-zero component in  $\tilde{\mathbf{F}}$  is the third one, corresponding to the correction of the energy flux.

Take learning  $\tilde{\mathbf{G}}, \mathbf{R}$  for example. At this point, we need a more concrete definition for the dynamics encoded in (12). The easiest way of doing this is to introduce certain numerical scheme for (12). We should emphasize that this scheme only serves to define the dynamics for the PDE. The machine learning model obtained is independent of the details of this scheme so long as it defines the same dynamics. We can think of a numerical scheme  $\mathcal{S}$  as an operator, which takes the flux function, the stencil, and numerical discretization parameters as input, and outputs the increment of the function values at the targeted point in time. For instance, in the case when  $D = 1$ , a simple example of  $\mathcal{S}$  may take the form

$$\hat{\mathbf{W}}_{j,n+1} - \mathbf{W}_{j,n} \approx \mathcal{S}[\tilde{\mathbf{G}}, \mathbf{R}](\mathbf{U}_{j-1,n}, \mathbf{U}_{j,n}, \mathbf{U}_{j+1,n}, \mathbf{W}_{j-1,n}, \mathbf{W}_{j,n}, \mathbf{W}_{j+1,n}; \Delta t, \Delta x, \varepsilon)$$

where  $j$  and  $n$  denote the spatial and temporal index respectively. In this case the tuple  $\mathcal{X} = (\mathbf{U}_{j-1,n}, \mathbf{U}_{j,n}, \mathbf{U}_{j+1,n}, \mathbf{W}_{j-1,n}, \mathbf{W}_{j,n}, \mathbf{W}_{j+1,n}, \mathbf{W}_{j,n+1})$  is an example of data needed. The loss function can be chosen as:

$$\mathbb{E}_{f \sim \mathcal{D}} \|\mathbf{W}_{j,n+1} - \mathbf{W}_{j,n} - \mathcal{S}(\mathbf{U}_{j-1,n}, \mathbf{U}_{j,n}, \mathbf{U}_{j+1,n}, \mathbf{W}_{j-1,n}, \mathbf{W}_{j,n}, \mathbf{W}_{j+1,n})\|^2.$$

Care should be exercised when choosing the numerical scheme, since the solutions of these systems may contain shocks. The task for learning  $\tilde{\mathbf{F}}$  can be formulated similarly based on the dynamics of  $\mathbf{U}$ . The details of the numerical scheme we use can be found in the supplementary material A.2.

**2.3. Data Exploration.** The quality of the proposed moment method depends on the quality of the data set  $\mathcal{D}$  that we use to train the model. Unlike conventional machine learning problems that rely on fixed data sets, here the construction of the data set is completely our own choice. In general our objective is to achieve greater accuracy with fewer training data by choosing the training data wisely. In this sense it is close to that of active learning [38]. To achieve this, an interactive algorithm is required between the augmentation of the data set and the learning process.

In this work we adopt the following strategy. One starts with a relatively small data set and uses it to learn the models. Then a new batch of solutions are generated for both the original kinetic model and the moment system. The error in the macroscopic variables  $\mathbf{U}$  is calculated as an indicator and the ones with large errors are added to the data set for the next round of learning. These two steps are repeated until convergence is achieved, which indicates that the phase space has been sufficiently explored. The whole scheme works as a closed loop and forms a self-learning process.

One key question is how to initialize the new batch of solutions. In principle we would like to initialize them so that at the end of the active learning process, the configurations that occur in practice have been explored sufficiently. Unfortunately at the moment, there are no precise mathematical principles that we can use as guidelines. This is certainly one issue that we will continue to investigate in the future. More details of the exploration procedure used can be found in the supplementary material A.5.

**2.4. Symmetries and Galilean Invariant Moments.** An important issue in building machine learning models is how to handle the symmetries in the system. The handling of translational, rotational and even permutational symmetries has been discussed in depth in the literature already [25, 39, 40, 41]. Besides these static symmetries, Boltzmann equation also possesses an important dynamic symmetry, the Galilean invariance. Specifically, for every  $\mathbf{u}' \in \mathbb{R}^D$ , define  $f'$  by  $f'(\mathbf{x}, \mathbf{u}, t) = f(\mathbf{x} - t\mathbf{u}', \mathbf{v} - \mathbf{u}', t)$ . If  $f$  is a solution of the Boltzmann equation, then so is  $f'$ . It is desirable that the reduced moment system also inherits such an invariance. Here we present a viable approach that achieves this goal.

The idea is to define the generalized moments  $\mathbf{W}_G$  (the subscript  $G$  signifies Galilean invariance) properly such that they are Galilean invariant. Given the velocity  $\mathbf{u}$  and temperature  $T$  of  $f$ , we modify the encoder to be

$$\mathbf{W}_G = \Psi_G(f) = \int_{\mathbb{R}^D} f(\mathbf{v}) \mathbf{w} \left( \frac{\mathbf{v} - \mathbf{u}}{\sqrt{T}} \right) d\mathbf{v}. \quad (13)$$

Note that the encoder  $\Psi_G$  now depends nonlinearly on the first and second moments of  $f$  and is invariant with respect to the choice of the Galilean reference frame.

Modeling the dynamics of  $\mathbf{W}_G$  becomes more subtle due to the spatial dependence in  $\mathbf{u}, T$ . Below for simplicity we will work with a discretized form of the dynamic model.

Suppose we want to model the dynamics of  $\mathbf{W}_{G,j}$  at the spatial grid point indexed by  $j$ . Integrating the Boltzmann equation against the generalized basis at this grid point gives

$$\partial_t \int_{\mathbb{R}^D} f \mathbf{w} \left( \frac{\mathbf{v} - \mathbf{u}_j}{\sqrt{T_j}} \right) d\mathbf{v} + \nabla_{\mathbf{x}} \cdot \int_{\mathbb{R}^D} f \mathbf{w} \left( \frac{\mathbf{v} - \mathbf{u}_j}{\sqrt{T_j}} \right) \mathbf{v}^T d\mathbf{v} = \int_{\mathbb{R}^D} \frac{1}{\varepsilon} Q(f) \mathbf{w} \left( \frac{\mathbf{v} - \mathbf{u}_j}{\sqrt{T_j}} \right) d\mathbf{v}. \quad (14)$$

The collision term on the right-hand side evaluated at the grid point  $j$  can still be approximated reasonably well by a function of  $(\mathbf{U}_j, \mathbf{W}_{G,j})$  only since there is no spatial interaction involved. However, after the discretization, the flux term above is going to depend not only on  $(\mathbf{U}, \mathbf{W}_G)$  but also on the basis quantity  $\mathbf{u}_j, T_j$  chosen in (14). This motivates us to consider the following approximate moment equation

$$\partial_t \mathbf{W}_G + \nabla_{\mathbf{x}} \cdot \mathbf{G}_G(\mathbf{U}, \mathbf{W}_G; \mathbf{U}_j) = \frac{1}{\varepsilon} \mathbf{R}_G(\mathbf{U}, \mathbf{W}_G). \quad (15)$$

Note that (15) is only meant to be used to model the dynamics of  $\mathbf{W}_{G,j}$ . To model the dynamics of  $\mathbf{W}_{G,j'}$  at another grid point  $j'$ , a different basis information  $\mathbf{U}_{j'}$  is provided. Given the moment equation (15), the loss functions for  $\mathbf{G}_G, \mathbf{R}_G$  can be defined in the same way as in Sec. 2.2. More discussion on the dynamics of Galilean invariant moment systems can be found in the supplementary material A.4.

One should also note that while preserving invariances is an important issue, it is not absolutely necessary to preserve such invariances exactly. In principle if the reduced dynamics is sufficiently accurate, all the invariances of the original system are satisfied approximately with similar accuracy.

**2.5. An End-To-End Learning Procedure.** The learning of the moment system introduced above is done through a two-step procedure for the moments and the dynamics of the moments. Here we present instead an end-to-end learning procedure.

For simplicity, we go back to the framework of Sections 2.1 and 2.2 (i.e. without specifying explicitly the Galilean invariance). The loss function for the autoencoder component is still defined as in (11). The functions in the moment equations are learned using the following loss functions, guided by (8) and its approximation (12). For  $\tilde{\mathbf{F}}$ , as discussed above, only the third component  $\tilde{\mathbf{F}}_3$ , the energy flux, needs to be considered. The corresponding loss function is given by

$$\mathbb{E}_{f \sim \mathcal{D}} \left\| \int_{\mathbb{R}^D} \frac{1}{2} f |\mathbf{v}|^2 \mathbf{v}^T d\mathbf{v} - (E + p) \mathbf{u}^T - \tilde{\mathbf{F}}_3(\mathbf{U}, \mathbf{W}) \right\|^2. \quad (16)$$

Similarly, the loss function for learning  $\tilde{\mathbf{G}}$  and  $\mathbf{R}$  can be written as

$$\mathbb{E}_{f \sim \mathcal{D}} \left\| \int_{\mathbb{R}^D} f \mathbf{w}(\mathbf{v}) \mathbf{v}^T d\mathbf{v} - \int_{\mathbb{R}^D} f_M(\mathbf{v}; \mathbf{U}) \mathbf{w}(\mathbf{v}) \mathbf{v}^T d\mathbf{v} - \tilde{\mathbf{G}}(\mathbf{U}, \mathbf{W}) \right\|^2, \quad (17)$$

$$\mathbb{E}_{f \sim \mathcal{D}} \left\| \int_{\mathbb{R}^D} Q(f) \mathbf{w}(\mathbf{v}) d\mathbf{v} - \mathbf{R}(\mathbf{U}, \mathbf{W}) \right\|^2. \quad (18)$$

Linearly combining eqs. (11) and (16) to (18) defines a loss function that allows us to learn the moment system in a single optimization step. The benefits of such a learning strategy are twofold. On one hand, training only requires data in terms of  $f$  instead of the evolution of  $f$ . The resulting paradigm becomes more like unsupervised learning rather than supervised learning since solving the Boltzmann equation becomes unnecessary. On the other hand, accuracy can potentially be improved since all the parameters are optimized jointly.

**2.6. An Alternative Direct Machine Learning Strategy.** A more straightforward machine learning approach is to stay at the level of the original hydrodynamic variables  $\mathbf{U}$  and directly learn a correction term for the Euler equations to approximate the dynamics of the Boltzmann equation:

$$\partial_t \mathbf{U} + \nabla_{\mathbf{x}} \cdot (\mathbf{F}_{\text{Euler}}(\mathbf{U}) + \tilde{\mathbf{F}}[\mathbf{U}(\cdot); \varepsilon]) = 0. \quad (19)$$

Here  $\tilde{\mathbf{F}}[\mathbf{U}(\cdot); \varepsilon]$  is a functional of  $\mathbf{U}(\cdot)$  that takes into account the information of  $\mathbf{U}$  in the whole space. It is quite straightforward to design machine learning models under this framework. For instance, assume that  $D = 1$ . One can discretize  $\mathbf{U}$  using  $N_x$  grid points and train a network to approximate  $\tilde{\mathbf{F}}$  in which the input is an  $N_x \times 4$  matrix representing  $\mathbf{U}$  and  $\varepsilon$ , and the output are the values of  $\tilde{\mathbf{F}}$  at the  $N_x$  grid points. In practice, to guarantee translational invariance and approximate locality, we choose a 1-D convolutional neural network with small convolution kernels. This approach is conceptually simple and easy to implement. Ideas like this have been used in various problems, including the turbulence models [25, 42, 43].

There are several problems with this. The first is that the approach does not offer any room for improving accuracy since no information can be used other than the instantaneous hydrodynamic variables. The second is that this procedure requires a specific discretization to begin with. The model obtained is tied with this discretization. We would like to have machine learning models that are more like PDEs. The third is that the models obtained is harder to interpret. For instance the role that the Knudsen number plays in the convolutional network is not as explicit as in the Boltzmann equation or the moment equation. In any case, it is our views that the moment system is a more appealing approach.

### 3. NUMERICAL RESULTS

As a first attempt, we report results for the methods introduced above using a BGK collision operator

$$Q(f) = f_M(\mathbf{v}; \mathbf{U}) - f.$$

The reason for choosing the BGK model is mainly for the convenience of data collection. The methodology introduced does not make use of the specific form of BGK at all and can be directly applied to more complicated kinetic models. We consider a one-dimensional problem on the spatial interval  $[-0.5, 0.5]$  with periodic boundary condition and time interval  $[0, 0.1]$ . Three different tasks are considered, termed *Task Wave*, *Task Mix*, and *Task MixInTransition* respectively. In the first two tasks the Knudsen number  $\varepsilon$  is constant across the whole domain, sampled from a log-uniform distribution on  $[-3, 1]$  respect to base 10, i.e.,  $\varepsilon$  takes values from  $10^{-3}$  to 10. For data exploration, the initial condition used in *Task Wave* consists of a few combination of waves randomly sampled from a probability distribution. For *Task Mix* the initial conditions contains a mixture of waves and shocks, both randomly sampled from their respective probability distributions. More details can be found in the supplementary material A.1. In *Task MixInTransition*, the initial condition is the same as in *Task Mix* but the Knudsen number is no longer constant in the spatial domain. Instead it varies from  $10^{-3}$  to 10. This is a toy model for transitional flows. We do not train any new models in *Task MixInTransition* but instead adopt the model learned from *Task Mix* directly to check its transferability. We use Implicit-Explicit (IMEX) scheme to generate the training data, with the spatial domain, time domain, and velocity domain been discretized using 100, 100, and 60 grid points respectively. In the reported results, *Task Wave* uses 100 paths as the training data set whereas *Task Mix* use 200 paths. In all the cases the test samples are sampled from the same distribution of the corresponding tasks. To evaluate the accuracy on the testing data, we consider two types of error measures for the macro quantities  $\mathbf{U}$ , the relative absolute error (RAE) and the relative squared error (RSE). More details of the tasks and data are provided in the supplementary material A.1.

We refer the models described in Sec. 2.1 and 2.2, Sec. 2.4, Sec. 2.5, Sec. 2.6 as MLMom, MLMomGalilean, MLMomE2E, DirectConv, respectively. Results of MLMom are always augmented by data exploration, unless specified. Other models do not use data exploration for ease of comparison. In all the numerical experiments presented in the main text, we always choose  $\mathbf{W}$  to be 6-dimensional. The result for choosing different number of moments is reported in the supplementary material A.6. Table 1 reports the relative errors of the different models on the testing data for the three tasks. The benefits brought by data exploration is clearly shown through

the comparison between the first two rows. MLMom with data exploration has a similar accuracy compared to MLMomGalilean. However, when the two models are trained on the data sets of the same size and distribution without data exploration, MLMomGalilean performs better than MLMom. The superiority of MLMomGalilean on data efficiency is not surprising since it better captures the intrinsic features of the original dynamical system. Fig. 2 shows some examples of the profiles of density, momentum, and energy at  $t = 0, 0.05, 0.1$  for the same initial condition, obtained by solving the kinetic equation, the Euler equations, and MLMom. More results can be found in the supplementary material A.6.

Model	<i>Wave</i>	<i>Mix</i>	<i>MixInTransition</i>
MLMom (no explor)	1.27(13), 1.60(35)	1.68(10), 2.35(12)	1.82(11), 2.49(11)
MLMom (explor)	0.85(10), 1.01(14)	1.25(5), 1.75(8)	1.55(4), 2.06(7)
MLMomGalilean	0.97(22), 1.11(23)	1.28(6), 1.85(10)	1.53(4), 2.11(8)
MLMomE2E	0.81(10), 0.97(11)	–	–
DirectConv	0.92(3), 1.16(6)	0.83(5), 1.13(9)	–

TABLE 1. Relative error (in percentages) of the different machine learning models for the three tasks. The first one in each cell denotes the relative absolute error (RAE) and the second denotes the relative squared error (RSE). The numbers in the parentheses denote the standard deviation of the last one or two digits computed from three independent runs. The results in the third column are obtained using the models learned in *Task Mix* directly.

While the generalized moments and moment equations are learned differently in *Task Wave* and *Task Mix* under the associated data distribution, in *Task MixInTransition* (the third column in Table 1), we use the same models learned from *Task Mix* directly without any further training. The fact that the relative error is similar to that in *Task Mix* indicates that the machine learning-based moment system has reliable transferability. On the contrary, while the model learned in *Task Wave* is accurate enough for that particular task, it is not sufficiently transferrable in general.

MLMomE2E has the best accuracy in *Task Wave* among all the models. Note that all the networks in MLMomE2E have the same structure as in MLMom, it seems that this improvement comes mainly from the end-to-end training process. However, when shocks are present, this model performs badly. For example, it may produce unphysical solutions. This should be due to the lack of any enforcement

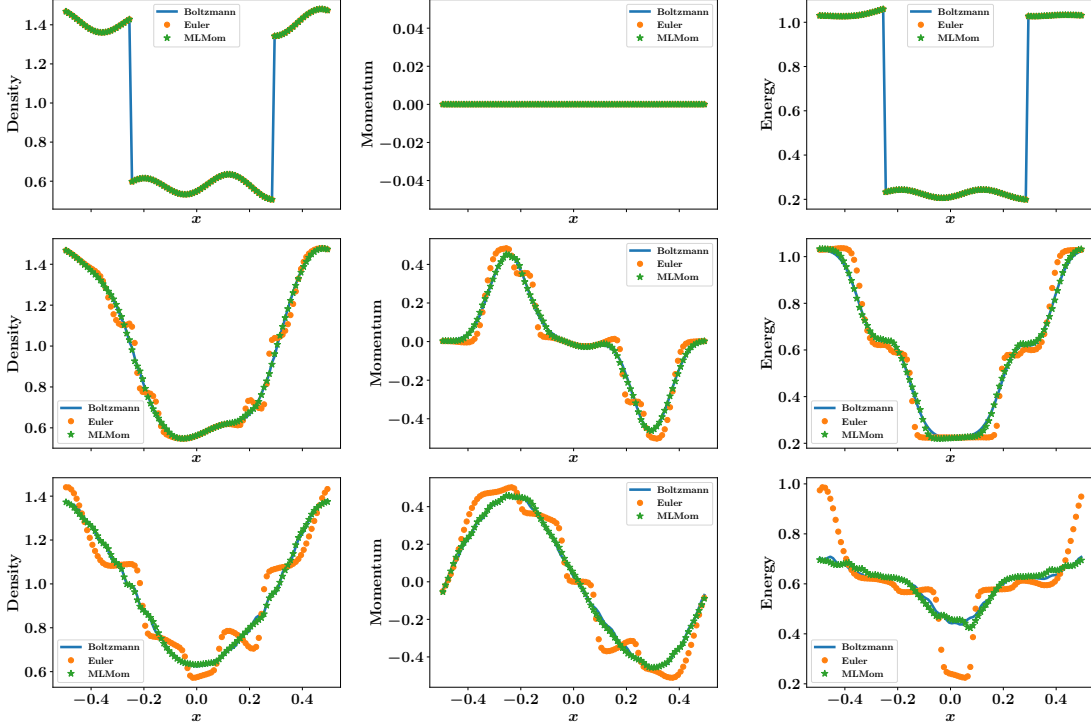


FIGURE 2. Sample profiles of density, momentum, and energy (from left to right) at  $t = 0, 0.05, 0.1$  (from top to bottom) in *Task Mix* with  $\varepsilon = 5.45$ , obtained from the kinetic equation, the Euler equations, and MLMom respectively.

of the entropy condition, either explicitly through the entropy function or implicitly through supervision from the dynamics of the kinetic equation. On the other hand, the existence of shocks is a special feature of the physical problem considered here. This issue disappears in most other physical systems and MLMomE2E should become a very attractive approach for those systems.

The accuracy of DirectConv is quite good for both *Task Wave* and *Task Mix*. However, the model obtained is tied to the specific discretization algorithm used and it is unclear how it can be used for other discretization schemes. The machine learning-based moment systems do not have this problem since they behave more like conventional PDEs. Fig. 3 illustrates the solutions of MLMom under the same initial condition as in *Task Wave* but different spatial discretizations.

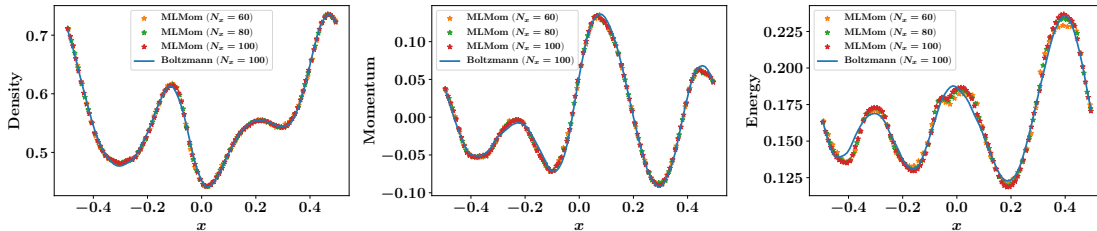


FIGURE 3. The solutions of MLMom at  $t = 0.1$  with the same initial profile in *Task Wave* with  $\varepsilon = 9.26$ , but different spatial discretizations

In Fig. 4 we display the log-log scatter plots of the relative error versus the Knudsen number  $\varepsilon$  for both *Task Wave* and *Task Mix*. One can see that the accuracy of the machine learning-based moment system is almost uniform across the whole regime, with the same computational cost. This stands in striking contrast to the conventional hydrodynamic models or DSMC method.

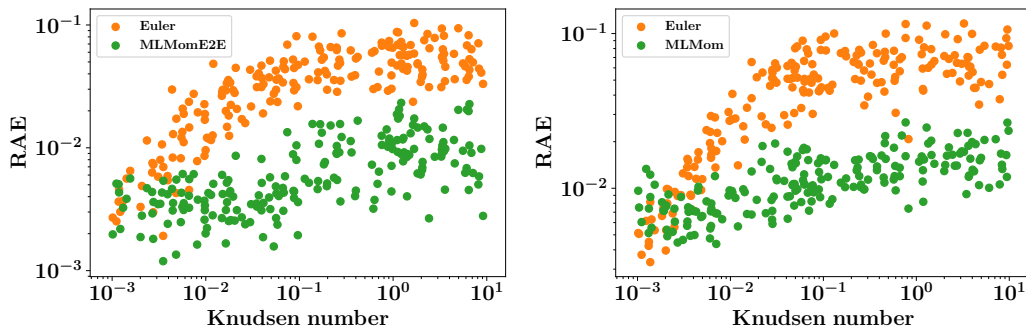


FIGURE 4. The log-log scatter plot of the relative error versus the Knudsen number  $\varepsilon$  for 200 testing paths in *Task Wave* (left) and *Task Mix* (right).

#### 4. DISCUSSION AND CONCLUSION

This paper presents a new framework for multi-scale modeling using machine learning in the absence of scale separation. We have put our emphasis on learning physical models, not just a particular algorithm. We have studied some of the main issues involved, including the importance of obeying physical constraints, actively learning, end-to-end models, etc. Our experience suggests that it is often advantageous to

respect physical constraints, but there is no need to sacrifice a lot of accuracy just to enforce them, since if we can model the dynamics accurately, the physical constraints are also satisfied with similar accuracy. Even though we still lack a proper mathematical framework to serve as guidelines, active learning is very important in order to ensure the validity of the model under different physical conditions. Regarding the end-to-end model, even though it did not perform satisfactorily for problem with shocks, we feel that it may very well be the most attractive approach in the more general cases since it seems most promising to derive uniform error bounds in this case.

Going back to the specific example we studied, kinetic equation with the BGK model, we presented an interpretable generalized moment system that works well in a wide range of Knudsen numbers. One can think of these models just like conventional PDEs, except that some of the terms in the fluxes and forcing terms are stored as subroutines. This is not very different from the conventional Euler's equation for complex gases where the equations of state are stored as look-up tables or sometimes subroutines. Regarding the three ingredients involved in learning the reduced models, namely, labeling the data, learning from the data, and exploring the data (as shown in Fig. 1), labeling the data is straightforward in this case: we just need to solve the BGK equation for some short period of time under different initial conditions. Data exploration is carried out using Monte Carlo sampling from some prescribed initial velocity distributions, and the picking of this initial velocity distribution is still somewhat ad hoc. The learning problem is the part that we have studied most carefully. We have explored and compared several different versions of machine learning models.

The immediate next step is to apply the principles presented here to other kinetic models such as the full Boltzmann equation in high dimension, kinetic models in plasma physics and kinetic models for complex fluids. We expect that most of these ideas can be directly applied to these systems. However, for each specific problem, the formulation of the reconstruction problem in the phase space and the starting point for learning the dynamic equations are different and can be quite non-trivial. Another issue is  $\varepsilon$  dependence of the reduced model. In this paper we adopted the simplest form of  $\varepsilon$  dependence, as shown in (12). This has the virtue of simplicity, particularly for transitional flows, but it may be the case that this is not the best form for achieving uniform accuracy. In addition, it introduces stiffness for small values of  $\varepsilon$  even though this seems to be a minor issue. More general  $\varepsilon$  dependence of the model needs to be investigated in the future.

## ACKNOWLEDGEMENT

The work presented here is supported in part by a gift to Princeton University from iFlytek and the ONR grant N00014-13-1-0338.

## REFERENCES

- [1] Weinan E, Bjorn Engquist, Xiantao Li, Weiqing Ren, and Eric Vanden-Eijnden. Heterogeneous multiscale methods: A review. *Communications in Computational Physics*, 2(3):367–450, 2007.
- [2] Weinan E. *Principles of Multiscale Modeling*. Cambridge University Press, 2011.
- [3] Stephen B. Pope. *Turbulent Flows*. Cambridge University Press, 2000.
- [4] Jiequn Han, Linfeng Zhang, Roberto Car, and Weinan E. Deep Potential: A general representation of a many-body potential energy surface. *Communications in Computational Physics*, 23(3):629–639, 2018.
- [5] Linfeng Zhang, Jiequn Han, Han Wang, Roberto Car, and Weinan E. Deep Potential Molecular Dynamics: A scalable model with the accuracy of quantum mechanics. *Physical Review Letters*, 120(14):143001, 2018.
- [6] Linfeng Zhang, De-Ye Lin, Han Wang, Roberto Car, and Weinan E. Active learning of uniformly accurate interatomic potentials for materials simulation. *Physical Review Materials*, 3(2):023804, 2019.
- [7] Harold Grad. On the kinetic theory of rarefied gases. *Communications on Pure and Applied Mathematics*, 2(4):331–407, 1949.
- [8] Claude Bardos, François Golse, and C. David Levermore. Fluid dynamic limits of kinetic equations II convergence proofs for the Boltzmann equation. *Communications on Pure and Applied Mathematics*, 46(5):667–753, 1993.
- [9] C. David Levermore. Moment closure hierarchies for kinetic theories. *Journal of Statistical Physics*, 83(5-6):1021–1065, 1996.
- [10] Graeme Austin Bird. *Molecular Gas Dynamics and the Direct Simulation of Gas Flows*. Clarendon press Oxford, 1994.
- [11] Francis J. Alexander and Alejandro L. Garcia. The direct simulation Monte Carlo method. *Computers in Physics*, 11(6):588–593, 1997.
- [12] Lorenzo Pareschi and Giovanni Russo. An introduction to Monte Carlo method for the Boltzmann equation. In *ESAIM: Proceedings*, volume 10, pages 35–75. EDP Sciences, 2001.
- [13] David Burnett. The distribution of velocities in a slightly non-uniform gas. *Proceedings of the London Mathematical Society*, 2(1):385–430, 1935.
- [14] Zhenning Cai, Yuwei Fan, and Ruo Li. Globally hyperbolic regularization of Grad’s moment system. *Communications on Pure and Applied Mathematics*, 67(3):464–518, 2014.
- [15] Zhenning Cai, Yuwei Fan, and Ruo Li. A framework on moment model reduction for kinetic equation. *SIAM Journal on Applied Mathematics*, 75(5):2001–2023, 2015.
- [16] Prabhu Lal Bhatnagar, Eugene P. Gross, and Max Krook. A model for collision processes in gases. I. Small amplitude processes in charged and neutral one-component systems. *Physical Review*, 94(3):511, 1954.
- [17] Maziar Raissi and George Em Karniadakis. Hidden physics models: Machine learning of non-linear partial differential equations. *Journal of Computational Physics*, 357:125–141, 2018.

- [18] Maziar Raissi, Paris Perdikaris, and George Em Karniadakis. Physics-informed neural networks: A deep learning framework for solving forward and inverse problems involving nonlinear partial differential equations. *Journal of Computational Physics*, 378:686–707, 2019.
- [19] Zichao Long, Yiping Lu, Xianzhong Ma, and Bin Dong. PDE-Net: Learning PDEs from data. In *Proceedings of the 35th International Conference on Machine Learning (ICML)*, 2018.
- [20] Zichao Long, Yiping Lu, and Bin Dong. PDE-Net 2.0: Learning PDEs from data with a numeric-symbolic hybrid deep network. *arXiv preprint arXiv:1812.04426*, 2018.
- [21] Samuel Rudy, Alessandro Alla, Steven L. Brunton, and J. Nathan Kutz. Data-driven identification of parametric partial differential equations. *SIAM Journal on Applied Dynamical Systems*, 18(2):643–660, 2019.
- [22] Kathleen P. Champion, Steven L. Brunton, and J. Nathan Kutz. Discovery of nonlinear multiscale systems: Sampling strategies and embeddings. *SIAM Journal on Applied Dynamical Systems*, 18(1):312–333, 2019.
- [23] Chao Ma, Jianchun Wang, and Weinan E. Model reduction with memory and the machine learning of dynamical systems. *Communications in Computational Physics*, 25(4):947–962, 2019.
- [24] Pantelis R. Vlachas, Wonmin Byeon, Zhong Y. Wan, Themistoklis P. Sapsis, and Petros Koumoutsakos. Data-driven forecasting of high-dimensional chaotic systems with long short-term memory networks. *Proceedings of the Royal Society A: Mathematical, Physical and Engineering Sciences*, 474(2213):20170844, 2018.
- [25] Julia Ling, Andrew Kurzawski, and Jeremy Templeton. Reynolds averaged turbulence modelling using deep neural networks with embedded invariance. *Journal of Fluid Mechanics*, 807:155–166, 2016.
- [26] Jian-Xun Wang, Jin-Long Wu, and Heng Xiao. Physics-informed machine learning approach for reconstructing Reynolds stress modeling discrepancies based on DNS data. *Physical Review Fluids*, 2(3):034603, 2017.
- [27] Qianxiao Li, Felix Dietrich, Erik M. Bollt, and Ioannis G. Kevrekidis. Extended dynamic mode decomposition with dictionary learning: A data-driven adaptive spectral decomposition of the koopman operator. *Chaos: An Interdisciplinary Journal of Nonlinear Science*, 27(10):103111, 2017.
- [28] Naoya Takeishi, Yoshinobu Kawahara, and Takehisa Yairi. Learning koopman invariant subspaces for dynamic mode decomposition. In *Advances in Neural Information Processing Systems (NIPS)*, pages 1130–1140, 2017.
- [29] Bethany Lusch, J. Nathan Kutz, and Steven L. Brunton. Deep learning for universal linear embeddings of nonlinear dynamics. *Nature communications*, 9(1):4950, 2018.
- [30] Kathleen Champion, Bethany Lusch, J. Nathan Kutz, and Steven L. Brunton. Data-driven discovery of coordinates and governing equations. *arXiv preprint arXiv:1904.02107*, 2019.
- [31] Carlo Cercignani. *Theory and Application of the Boltzmann Equation*. Scottish Academic Press, 1975.
- [32] Sydney Chapman and Thomas George Cowling. *The Mathematical Theory of Non-uniform Gases: An Account of the Kinetic Theory of Viscosity, Thermal Conduction and Diffusion in Gases*. Cambridge University Press, 1990.
- [33] Takaaki Nishida. Fluid dynamical limit of the nonlinear Boltzmann equation to the level of the compressible Euler equation. *Communications in Mathematical Physics*, 61(2):119–148, 1978.

- [34] Russel E. Caflisch. The fluid dynamic limit of the nonlinear Boltzmann equation. *Communications on Pure and Applied Mathematics*, 33(5):651–666, 1980.
- [35] François Bouchut, François Golse, and Mario Pulvirenti. *Kinetic equations and asymptotic theory*. Elsevier, 2000.
- [36] Geoffrey E. Hinton and Ruslan R. Salakhutdinov. Reducing the dimensionality of data with neural networks. *Science*, 313(5786):504–507, 2006.
- [37] Ian Goodfellow, Yoshua Bengio, and Aaron Courville. *Deep Learning*. MIT press, 2016.
- [38] Burr Settles. Active learning literature survey. Technical report, University of Wisconsin-Madison Department of Computer Sciences, 2009.
- [39] Manzil Zaheer, Satwik Kottur, Siamak Ravanbakhsh, Barnabas Poczos, Ruslan R. Salakhutdinov, and Alexander J. Smola. Deep sets. In *Advances in Neural Information Processing Systems (NIPS)*, pages 3391–3401, 2017.
- [40] Linfeng Zhang, Jiequn Han, Han Wang, Wissam Saidi, Roberto Car, and Weinan E. End-to-end symmetry preserving inter-atomic potential energy model for finite and extended systems. In *Advances in Neural Information Processing Systems*, pages 4436–4446, 2018.
- [41] Michael Eickenberg, Georgios Exarchakis, Matthew Hirn, Stéphane Mallat, and Louis Thiry. Solid harmonic wavelet scattering for predictions of molecule properties. *The Journal of chemical physics*, 148(24):241732, 2018.
- [42] Karthik Duraisamy, Gianluca Iaccarino, and Heng Xiao. Turbulence modeling in the age of data. *Annual Review of Fluid Mechanics*, 51:357–377, 2019.
- [43] Enrico Fonda, Ambrish Pandey, Jörg Schumacher, and Katepalli R. Sreenivasan. Deep learning in turbulent convection networks. *Proceedings of the National Academy of Sciences*, 116(18):8667–8672, 2019.
- [44] Francis Filbet and Shi Jin. A class of asymptotic-preserving schemes for kinetic equations and related problems with stiff sources. *Journal of Computational Physics*, 229(20):7625–7648, 2010.
- [45] Eleuterio F. Toro. *The HLL and HLLC Riemann Solvers*, pages 293–311. Springer Berlin Heidelberg, Berlin, Heidelberg, 1997.
- [46] Clawpack Development Team. Clawpack software, 2018. Version 5.5.0.
- [47] Kyle T. Mandli, Aron J. Ahmadi, Marsha Berger, et al. Clawpack: building an open source ecosystem for solving hyperbolic PDEs. *PeerJ Computer Science*, 2:e68, 2016.
- [48] Randall J. LeVeque. *Finite Volume Methods for Hyperbolic Problems*. Cambridge University Press, 2002.
- [49] Zhenning Cai and Ruo Li. Numerical regularized moment method of arbitrary order for Boltzmann-BGK equation. *SIAM Journal on Scientific Computing*, 32(5):2875–2907, 2010.
- [50] Zhenning Cai, Ruo Li, and Yanli Wang. An efficient NR $xx$  method for Boltzmann-BGK equation. *Journal of Scientific Computing*, 50(1):103–119, 2012.
- [51] Zhenning Cai, Yuwei Fan, and Ruo Li. Globally hyperbolic regularization of Grad’s moment system in one dimensional space. *Communications in Mathematical Sciences*, 11(2):547–571, 2013.
- [52] Zhenning Cai, Ruo Li, and Zhonghua Qiao. Globally hyperbolic regularized moment method with applications to microflow simulation. *Computers & Fluids. An International Journal*, 81:95–109, 2013.

- [53] Sergey Ioffe and Christian Szegedy. Batch normalization: accelerating deep network training by reducing internal covariate shift. In *Proceedings of the 32nd International Conference on Machine Learning (ICML)*, 2015.
- [54] Diederik Kingma and Jimmy Ba. Adam: a method for stochastic optimization. In *Proceedings of the International Conference on Learning Representations (ICLR)*, 2015.
- [55] Kaiming He, Xiangyu Zhang, Shaoqing Ren, and Jian Sun. Deep residual learning for image recognition. In *Proceedings of the IEEE Conference on Computer Vision and Pattern Recognition*, 2016.

### SUPPLEMENTARY MATERIAL

**A.1. Tasks and Data.** We consider 1-D domain  $[-0.5, 0.5]$  with periodic boundary condition. We put down a uniform grid of 100 grid points. The time interval considered is  $[0, 0.1]$  with time step size 0.001. The velocity domain is truncated to  $[-10, 10]$  and discretized using 60 nodes according to the Gauss-Legendre quadrature rule. In *Task Wave* and *Task Mix* the Knudsen number  $\varepsilon$  is sampled from a log-uniform distribution on  $[-3, 1]$  respect base 10, i.e.,  $\varepsilon$  takes values from  $10^{-3}$  to 10, constant across the domain. We consider two types of initial conditions in all the three tasks.

For *Task Wave* the initial condition  $f_{wave}$  is sampled from a mixture of two local Maxwellian distributions. Two macroscopic functions  $\mathbf{U}_1, \mathbf{U}_2$  are firstly sampled from sine waves

$$\begin{cases} \rho(x, 0) = a_\rho \sin(2k_\rho \pi x / L + \psi_\rho) + b_\rho, \\ u(x, 0) = 0, \\ T(x, 0) = a_T \sin(2k_T \pi x / L + \psi_T) + b_T. \end{cases}$$

Here we assume  $a_\rho, \psi_\rho, b_\rho$  are random variables sampled from the uniform distributions on  $[0.2, 0.3]$ ,  $[0, 2\pi]$ ,  $[0.5, 0.7]$ , respectively.  $k_\rho$  is the random integer sampled uniformly from the set  $\{1, 2, 3, 4\}$ .  $a_T, \psi_T, b_T, k_T$  in  $T(\cdot, 0)$  are independent and identically distributed random variables as their counterparts in the function  $\rho(\cdot, 0)$ . Finally, two local Maxwellian distributions are randomly mixed through

$$f_{wave} = \frac{\alpha_1 f_M(\mathbf{v}; \mathbf{U}_1) + \alpha_2 f_M(\mathbf{v}; \mathbf{U}_2)}{\alpha_1 + \alpha_2 + 10^{-6}},$$

in which  $\alpha_1, \alpha_2$  are two random variables sampled from the uniform distribution on  $[0, 1]$ .

For *Task Mix* the initial condition  $f_{mix}$  is sampled from a random superposition of two functions,  $f_{wave}$  as defined above and  $f_{shock}$ .  $f_{shock}$  is also a point-wise local Maxwellian, except that the macroscopic functions  $\mathbf{U}$  are made up from some Riemann problems. Consider the Riemann problem in which  $\rho_L, T_L$  are two independent

random variables sampled from the uniform distribution on  $[1, 2]$ ,  $\rho_R, T_R$  are two independent random variables sampled from the uniform distributions on  $[0.55, 0.9]$ , and  $u_L, u_R$  are 0. The initial condition  $f_{shock}$  then has the form

$$\begin{cases} \rho(x, 0), u(x, 0), T(x, 0) = \rho_L, u_L, T_L, & x \in [-0.5, x_1] \text{ or } x \in [x_2, 0.5], \\ \rho(x, 0), u(x, 0), T(x, 0) = \rho_R, u_R, T_R, & x \in (x_1, x_2), \end{cases}$$

or

$$\begin{cases} \rho(x, 0), u(x, 0), T(x, 0) = \rho_R, u_R, T_R, & x \in [-0.5, x_1] \text{ or } x \in [x_2, 0.5], \\ \rho(x, 0), u(x, 0), T(x, 0) = \rho_L, u_L, T_L, & x \in (x_1, x_2), \end{cases}$$

where  $x_1, x_2$  are two random variables sampled from the uniform distributions on  $[-0.3, -0.1]$  and  $[0.1, 0.3]$ . Finally, we linearly combine two initial conditions to obtain

$$f_{mix} = \alpha f_{wave} + (1 - \alpha) f_{shock},$$

where  $\alpha$  is a random variable sampled from the uniform distribution on  $[0.2, 0.6]$ .

For *Task MixInTransition* the initial condition is the same as in *Task Mix*. The values of  $\varepsilon$  vary from  $10^{-3}$  to 10 in the domain, similar to the one used in [44],

$$\varepsilon(x) = 10^{-3} + 5(\tanh(1 + 11(x - x_0)) + \tanh(1 - 11(x - x_0))),$$

where  $x_0$  is sampled from the uniform distribution on  $[-0.2, 0.2]$ . This is where the Knudsen number is at its maximum. The sample profiles of density, energy, and Knudsen number in *Task MixInTransition* are shown in Fig. 5.

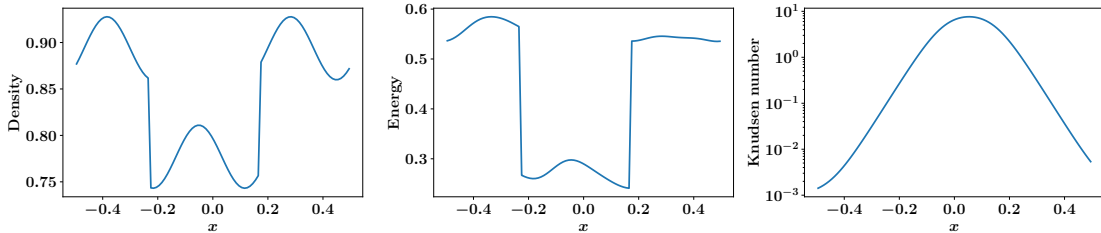


FIGURE 5. Sample profiles of density, energy, and Knudsen number in *Task MixInTransition*.

We compute two types of error, the relative absolute error (RAE) and the relative squared error (RSE), to measure the accuracy of different models. By a slight abuse of notation, we consider  $N$  independent profiles of conserved quantities,  $\mathbf{U}^{(i)}, \hat{\mathbf{U}}^{(i)}$ ,  $i = 1, \dots, N$ , computed from the kinetic equation and the machine learning-based

model respectively. Assume that each profile is discretized using  $N_x$  grid points indexed by  $j$ . We define

$$\begin{aligned} \text{RAE} &= \frac{1}{2NN_x} \sum_{i,j} \frac{|\mathbf{U}_j^{(i)} - \hat{\mathbf{U}}_j^{(i)}|}{|\mathbf{U}_j^{(i)}|}, \\ \text{RSE} &= \sqrt{\frac{\sum_{i,j} (\mathbf{U}_j^{(i)} - \hat{\mathbf{U}}_j^{(i)})^2}{\sum_{i,j} (\mathbf{U}_j^{(i)})^2}}. \end{aligned}$$

There are other ways to measure the accuracy, but our experience suggests that the overall behavior is quite independent of the accuracy measure that we use.

**A.2. Numerical Scheme.** Here we introduce in detail the numerical scheme  $\mathcal{S}$  used when learning the moment closure. This enters into the concrete form of the loss function for the dynamics of  $\mathbf{U}$  and  $\mathbf{W}$ . Recall the dynamic equation

$$\begin{cases} \partial_t \mathbf{U} + \nabla_{\mathbf{x}} \cdot [\mathbf{F}_{\text{Euler}}(\mathbf{U}) + \tilde{\mathbf{F}}(\mathbf{U}, \mathbf{W})] = 0, \\ \partial_t \mathbf{W} + \nabla_{\mathbf{x}} \cdot [\mathbf{G}(\mathbf{U}, \mathbf{W})] = \frac{1}{\varepsilon} \mathbf{R}(\mathbf{U}, \mathbf{W}), \end{cases} \quad (20)$$

where  $\mathbf{G}(\mathbf{U}) = \mathbf{G}_0(\mathbf{U}) + \tilde{\mathbf{G}}(\mathbf{U}, \mathbf{W})$ , as explained in Sec. 2.2. Applying the classical finite volume discretization to (20), we get

$$\begin{cases} \hat{\mathbf{U}}_{j,n+1} = \mathbf{U}_{j,n} - \frac{\Delta t}{\Delta x} ((\mathbf{F}_{\text{Euler}})_{j+1/2,n} - (\mathbf{F}_{\text{Euler}})_{j-1/2,n}) - \frac{\Delta t}{\Delta x} (\tilde{\mathbf{F}}_{j+1/2,n} - \tilde{\mathbf{F}}_{j-1/2,n}), \\ \hat{\mathbf{W}}_{j,n+1} = \mathbf{W}_{j,n} - \frac{\Delta t}{\Delta x} (\mathbf{G}_{j+1/2,n} - \mathbf{G}_{j-1/2,n}) + \frac{\Delta t}{\varepsilon} \mathbf{R}(\mathbf{U}_{j,n}, \mathbf{W}_{j,n}), \end{cases} \quad (21)$$

where  $\hat{\mathbf{U}}_{j,n+1}$  and  $\hat{\mathbf{W}}_{j,n+1}$  denote the one-step solution of the machine learning-based model at the spatial grid point  $j$  and time step  $n+1$ . This is a conservative scheme with first order accuracy in both time and space.

For  $(\mathbf{F}_{\text{Euler}})_{j+1/2,n}$ , any classical numerical scheme for solving the Euler equations can be applied since there is no parameter to optimize. In our implementation, we choose the 1-D HLLC Riemann solver [45] with entropy fix implemented in the open source package Clawpack [46, 47, 48].

Regarding the fluxes  $\tilde{\mathbf{F}}_{j+1/2,n}$  and  $\mathbf{G}_{j+1/2,n}$ , we choose a generalized Lax-Friedrichs scheme based on a three-point stencil,

$$\begin{aligned} \begin{pmatrix} \tilde{\mathbf{F}}_{j+1/2,n} - \tilde{\mathbf{F}}_{j-1/2,n} \\ \mathbf{G}_{j+1/2,n} - \mathbf{G}_{j-1/2,n} \end{pmatrix} &= \begin{pmatrix} \tilde{\mathbf{F}}(\mathbf{U}_{j+1,n}, \mathbf{W}_{j+1,n}) - \tilde{\mathbf{F}}(\mathbf{U}_{j-1,n}, \mathbf{W}_{j-1,n}) \\ \mathbf{G}(\mathbf{U}_{j+1,n}, \mathbf{W}_{j+1,n}) - \mathbf{G}(\mathbf{U}_{j-1,n}, \mathbf{W}_{j-1,n}) \end{pmatrix} \\ &\quad - \begin{pmatrix} A_U(\mathbf{U}_{j+1,n} - 2\mathbf{U}_{j,n} + \mathbf{U}_{j-1,n}) \\ A_W(\mathbf{W}_{j+1,n} - 2\mathbf{W}_{j,n} + \mathbf{W}_{j-1,n}) \end{pmatrix}, \end{aligned} \quad (22)$$

where the constants  $A_U, A_W$  are the numerical viscosity coefficients. We optimize these constants during training such that a suitable strength of the numerical viscosity can be found for the machine-learned fluxes.

Combining (21) and (22), we see that the one-step output of the numerical scheme  $\mathcal{S}$  is continuous respect to all the parameters. Hence we can use stochastic gradient descent to optimize them.

**A.3. Hyperbolic Moment Equation.** In this section, we briefly discuss the conventional moment system (see for example [14, 15]). The starting point is to expand, at each point in  $(\mathbf{x}, t)$ , the phase space density  $f$  in Hermite polynomials in  $\mathbf{v}$  that are normalized by the macroscopic variables  $\mathbf{u}(\mathbf{x}, t), T(\mathbf{x}, t)$ . The expansion is truncated at a predefined order. This truncated system of equations for the expansion coefficients is the moment system. A regularization term is added to the equation for the highest order to ensure that the moment system is hyperbolic. We refer the readers to [49, 50, 51, 52] for more details of this approach.

The machine learning-based approach shares a lot in common with this more conventional approach: both attempt to solve the kinetic equation accurately; the issues of Galilean invariance are similar; etc. However, there is one important difference: While the approach mentioned above can be viewed as a spectral method for the  $\mathbf{v}$  component of the variables, the machine learning-based presented here is more like an adaptive basis function approach. In many ways, adaptivity is one of the key features of the machine learning-based approach.

In order to get some ideas about quantitative comparison, we implemented the algorithm for solving the hyperbolic moment equation according to [52] and tested it on all the three tasks considered in the paper. We use 200 grid points in the spatial domain and 9 moments in total. The relative RAE and RSE in percentages are 2.36(3), 3.07(4) (*Task Wave*), 2.13(2), 3.25(17) (*Task Mix*), 2.11(7), 3.39(8) (*Task MixInTransition*). This is slightly worse than the results for the machine learning-based models. It should be pointed out that it is difficult to compare these results directly with the proposed machine learning-based moment system since there are

a lot of factors that contribute to the accuracy. Nevertheless, we feel that for more challenging problems such as the kinetic models represented by DSMC, the advantage of the machine learning-based approach will be more striking.

**A.4. Galilean Invariant Dynamics.** The first step of MLMomGalilean, finding generalized moments  $\mathbf{W}_G$ , naturally obeys Galilean invariance. It is more subtle for the dynamics of  $\mathbf{W}_G$  to obey Galilean invariance since the associated PDE has additional convection terms involving  $\nabla_{\mathbf{x}}\mathbf{u}, \nabla_{\mathbf{x}}T$  compared to (9). The simplest approximate solution to this problem is to introduce some spatial dependence into the PDE models.

As discussed in Sec. 2.4, when considering the local dynamics of  $\mathbf{W}_{G,j}$  at the grid point  $j$ , the exact flux function should be

$$\int_{\mathbb{R}^D} f(\mathbf{v})\mathbf{w}\left(\frac{\mathbf{v}-\mathbf{u}_j}{\sqrt{T_j}}\right)\mathbf{v}^T d\mathbf{v}.$$

We need to approximate this quantity in the form of  $\mathbf{G}_G(\mathbf{U}, \mathbf{W}_G; \mathbf{U}_j)$  as proposed in (15), a function of the macroscopic variables  $\mathbf{U}, \mathbf{W}_G$ , with the basis information  $\mathbf{U}_j$  provided as well. Meanwhile, we would like to have an alternative expression similar to the flux terms in (12) in order to reduce the variance during training. Note that in this setting  $\mathbf{G}_0(\mathbf{U})$  is much more expensive to compute than its counterpart in MLMom since the Gauss-Legendre quadrature rule now requires evaluating  $\mathbf{w}(\mathbf{v})$  at different sets of the grid points for each single batch of data, due to the nonlinear dependence on  $\mathbf{u}$  and  $T$ . Instead we consider another decomposition of the flux function

$$\begin{aligned} & \int_{\mathbb{R}^D} f\mathbf{w}\left(\frac{\mathbf{v}-\mathbf{u}_j}{\sqrt{T_j}}\right)\mathbf{v}^T d\mathbf{v} \\ &= \int_{\mathbb{R}^D} f\mathbf{w}\left(\frac{\mathbf{v}-\mathbf{u}_j}{\sqrt{T_j}}\right)(\mathbf{v}-\mathbf{u})^T d\mathbf{v} + \left(\int_{\mathbb{R}^D} f\mathbf{w}\left(\frac{\mathbf{v}-\mathbf{u}_j}{\sqrt{T_j}}\right) d\mathbf{v}\right)\mathbf{u}^T \\ &\approx \int_{\mathbb{R}^D} f\mathbf{w}\left(\frac{\mathbf{v}-\mathbf{u}_j}{\sqrt{T_j}}\right)(\mathbf{v}-\mathbf{u})^T d\mathbf{v} + \left(\int_{\mathbb{R}^D} f\mathbf{w}\left(\frac{\mathbf{v}-\mathbf{u}}{\sqrt{T}}\right) d\mathbf{v}\right)\mathbf{u}^T \\ &= \int_{\mathbb{R}^D} f\mathbf{w}\left(\frac{\mathbf{v}-\mathbf{u}_j}{\sqrt{T_j}}\right)(\mathbf{v}-\mathbf{u})^T d\mathbf{v} + \mathbf{W}_G\mathbf{u}^T. \end{aligned}$$

Here the approximation  $\mathbf{u} \approx \mathbf{u}_j$  in the second term is made on the grounds that the flux above is used only locally around the grid point  $j$ . If we also assume  $\mathbf{u} \approx \mathbf{u}_j$

in the first term above, it will be equivalent to  $\int_{\mathbb{R}^D} f(\mathbf{v} + \mathbf{u}) \mathbf{w}(\frac{\mathbf{v}}{\sqrt{T}}) \mathbf{v}^T d\mathbf{v}$ . Such an expression is consistent with our consideration of the Galilean invariance because it only depends on the shape of the phase density rather than the choice of the Galilean reference frame. The above decomposition finally motivates us to write

$$\mathbf{G}_G(\mathbf{U}, \mathbf{W}_G; \mathbf{U}_j) = \tilde{\mathbf{G}}_G(\mathbf{U}, \mathbf{W}_G; \mathbf{U}_j) + \mathbf{W}_G \mathbf{u}^T, \quad (23)$$

where  $\tilde{\mathbf{G}}_G$  is the neural network to be optimized. This ensures that the dynamics of  $\mathbf{W}_G$  also obeys Galilean invariance approximately.

### A.5. Learning of Neural Networks.

**MLMom and MLMomGalilean.** We use the same architecture for the neural networks used in MLMom and MLMomGalilean. The input is always the concatenation of all the variables listed. For the autoencoder, the basis function  $\mathbf{w}$  of the encoder in (10) is represented by a fully-connected neural network with two hidden-layers and  $3M$  hidden nodes in each layer (recall  $M$  denotes the dimension of the generalized moments  $\mathbf{W}$ ). We use the same technique as in Batch Normalization [53] to normalize the output within each data batch to ensure zero mean and unit variance. It is observed that this operation improves the stability of training. The function  $h$  in the decoder is represented by another neural network with two hidden layers, whose widths are  $2M$  and  $M$ , respectively. The activation function is chosen to be the softplus function.  $\lambda_\eta$  in (11) is chosen to be 0.01. The Adam optimizer [54] is used with learning rate 0.001 and batch size 100 for training the autoencoder. Usually the autoencoder is trained for 60-120 epochs, depending on the type of initial condition and the size of the data set.

For the moment closure in (12),  $\tilde{\mathbf{F}}$  is modeled by a neural network with two hidden-layers and 32 hidden nodes per layer,  $\tilde{\mathbf{G}}$  and  $\mathbf{R}$  are modeled by two neural networks both with 3 hidden-layers and 64 hidden nodes in each layer. All three neural networks use the residual connection [55] in the hidden layers. Again softplus is used as the activation function. When building the loss function, we have two separate terms: one for  $\tilde{\mathbf{F}}$  and the other for  $\tilde{\mathbf{G}}$  and  $\mathbf{R}$ , as described in Sec. 2.2. We use a weighted sum of the two terms as our loss function, with weight 100 and 0.001, respectively. An Adam optimizer is employed to train the networks. The learning rate starts from 0.01 and decays exponentially to 0.001. Training takes 20 epochs with batch size 256.

**MLMomE2E.** For MLMomE2E, we use the exact same architecture for all the networks as in MLMom and MLMomGalilean in both the autoencoder and the moment closure. The single loss function is a linear combination of (11)(16)(17)(18) with

weights 1, 10,  $0.001/SS_1$ ,  $0.001/SS_2$ . Here  $SS_1$  and  $SS_2$  denote the total sum of squares in the associated regression problem

$$SS_1 = \mathbb{E}_{f \sim \mathcal{D}} \left\| \int_{\mathbb{R}^D} f \mathbf{w}(\mathbf{v}) \mathbf{v}^T d\mathbf{v} - \int_{\mathbb{R}^D} f_M(\mathbf{v}; \mathbf{U}) \mathbf{w}(\mathbf{v}) \mathbf{v}^T d\mathbf{v} \right\|^2,$$

$$SS_2 = \mathbb{E}_{f \sim \mathcal{D}} \left\| \int_{\mathbb{R}^D} Q(f) \mathbf{w}(\mathbf{v}) d\mathbf{v} \right\|^2.$$

It is equivalent to optimizing the relative loss instead of absolute loss. Noting that these two terms actually depend on the encoder, we use the statistics within the batch during training to approximate them. An Adam optimizer is used for 90 epochs with batch size 100. The learning rate is constant during each 30-epoch periods, decreasing from 0.005 to 0.001, and then to 0.0005.

**DirectConv.** As described in Sec. 2.6, we use a 1-D convolutional neural network to represent the third component of functional  $\tilde{\mathbf{F}}$ . The input of the network contains 4 channels of length  $N_x$ . The architecture of the network can be expressed

$$\begin{array}{ccccccc} N_x \times 4 & \xrightarrow{Conv} & N_x \times 40 & \xrightarrow{Pooling} & N_x/2 \times 40 & \xrightarrow{Conv} & N_x/2 \times 40 \\ \xrightarrow{Pooling} & N_x/4 \times 40 & \xrightarrow[Res]{Conv} & N_x/4 \times 40 & \xrightarrow[Res]{Conv} & N_x/4 \times 40 & \xrightarrow{Conv} & N_x/4 \times 3 \\ \xrightarrow{Deconv} & N_x/2 \times 3 & \xrightarrow{Deconv} & N_x \times 1 & & & & \end{array}$$

where *Conv* represents 1-D convolution with kernel size 4 and periodic padding followed by a softplus activation, *Pooling* is done by max pooling, *Res* means a residual connection in the layer, and *Deconv* means a 1-D deconvolution operation with kernel size 4 and stride 2. The network is trained by an Adam optimizer with batch size 50 and learning rate exponentially decreasing from 0.001 to 0.0002. Training is run for 5000 epochs.

**Data Exploration.** For *Task Wave*, an autoencoder is initially trained for 120 epochs with a data set containing 50 paths, sampled from the distribution of the initial profiles. Then, 5 loops of exploration is done as follows. In each loop, 100 new paths are evaluated by both the original kinetic model and the moment system, in which 10 paths with the largest errors are added to the data set, then the autoencoder is retrained for another 20 epochs on the new data set. Finally the data set contains 100 paths, the same as in the case without data exploration. For *Task Mix* the autoencoder is initially trained for 90 epochs on 100 paths, before 5 loops of data exploration. In each loop, 20 paths with the largest errors from 200 randomly sampled paths are added to the data set, and then the autoencoder is retrained for

15 epochs. The final data set contains 200 paths, the same as in the case without data exploration. The autoencoders, fluxes, and production terms used in *Task MixInTransition* are the same as *Task Mix*. No additional training was used.

It is worth mentioning that in the current implementation of data exploration, the cost of generating truthful micro-scale data is not directly reduced because it is needed in evaluating the prediction error of the new data in the exploration stage. There are various ways to fix this problem, for instance, by using the variance from the predictions of an ensemble of networks optimized independently as an indicator of the error in the exploration, as was done in [6]. This is left for future work.

**A.6. Additional Results.** Fig. 6 plots all six generalized moment functions obtained in MLMomGalilean for *Task Mix*. As we can see they are all well-behaved functions. If we train MLMomGalilean for *Task Mix* using 3 or 9 generalized moments, the resulted RAE and RSE are 2.00(12), 3.03(30) and 1.27(5) and 1.92(18) respectively. Comparing these results with Table 1, we see that choosing 6 additional generalized moments is a suitable trade-off between accuracy and efficiency given the sizes of the networks and the data sets used in the current experiments.

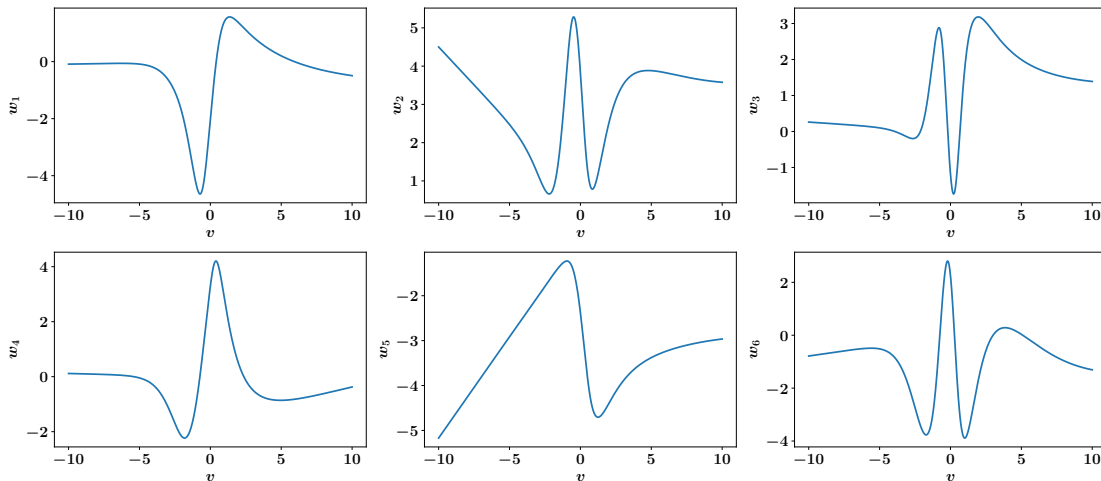


FIGURE 6. Optimized encoder  $\mathbf{w}(\mathbf{v})$  in MLMomGalilean, as the generalized moment functions for *Task Mix*.

Fig. 7 shows the growth of the relative errors for the solutions of the Euler equations and machine learning-based moment system on 200 new paths in *Task Wave*, *Task Mix*, and *Task MixInTransition*.

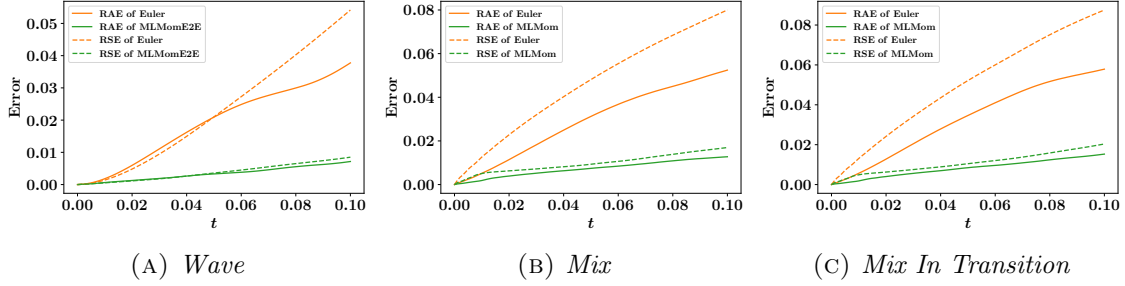


FIGURE 7. The growth of the relative error as a function of time for 200 new paths in *Task Wave*, *Task Mix*, and *Task MixInTransition*.

Fig. 8 and Fig. 9 illustrate two sample profiles of density, momentum, and energy in *Task Wave* and *Task MixInTransition*, obtained from the kinetic equation, the Euler equations, and the machine learning-based moment system.

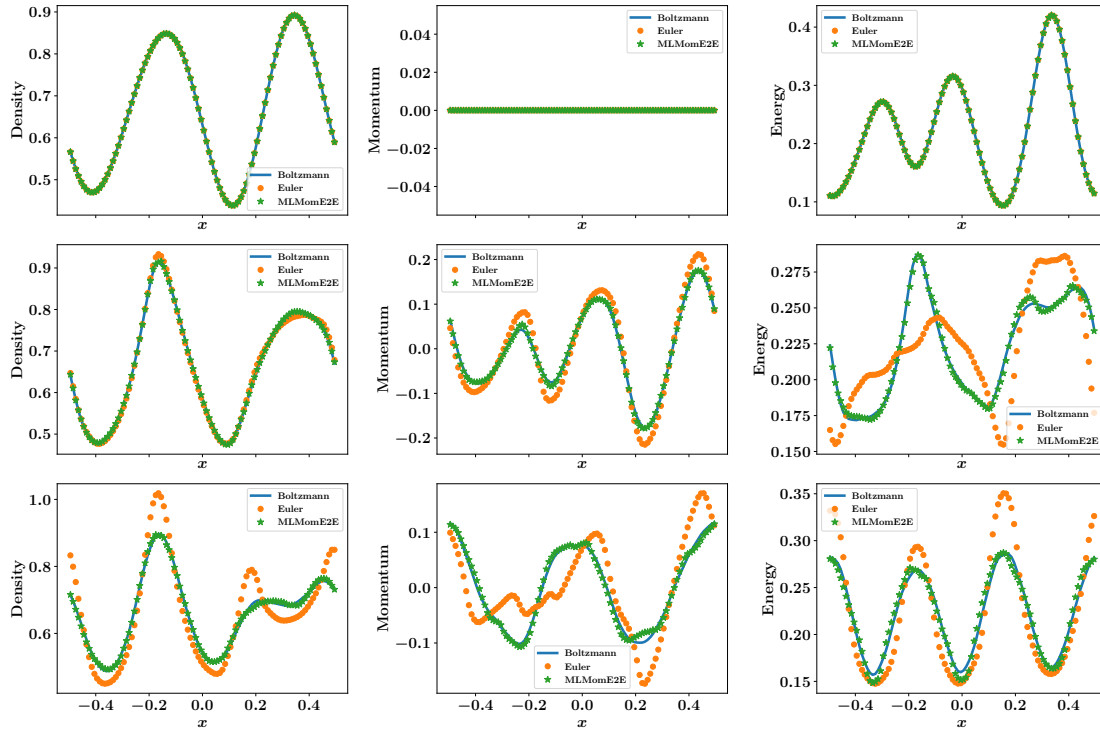


FIGURE 8. Sample profiles of density, momentum, and energy (from left to right) at  $t = 0, 0.05, 0.1$  (from top to bottom) in *Task Wave* with  $\varepsilon = 9.32$ , obtained from the kinetic equation, the Euler equations, and MLMomE2E.

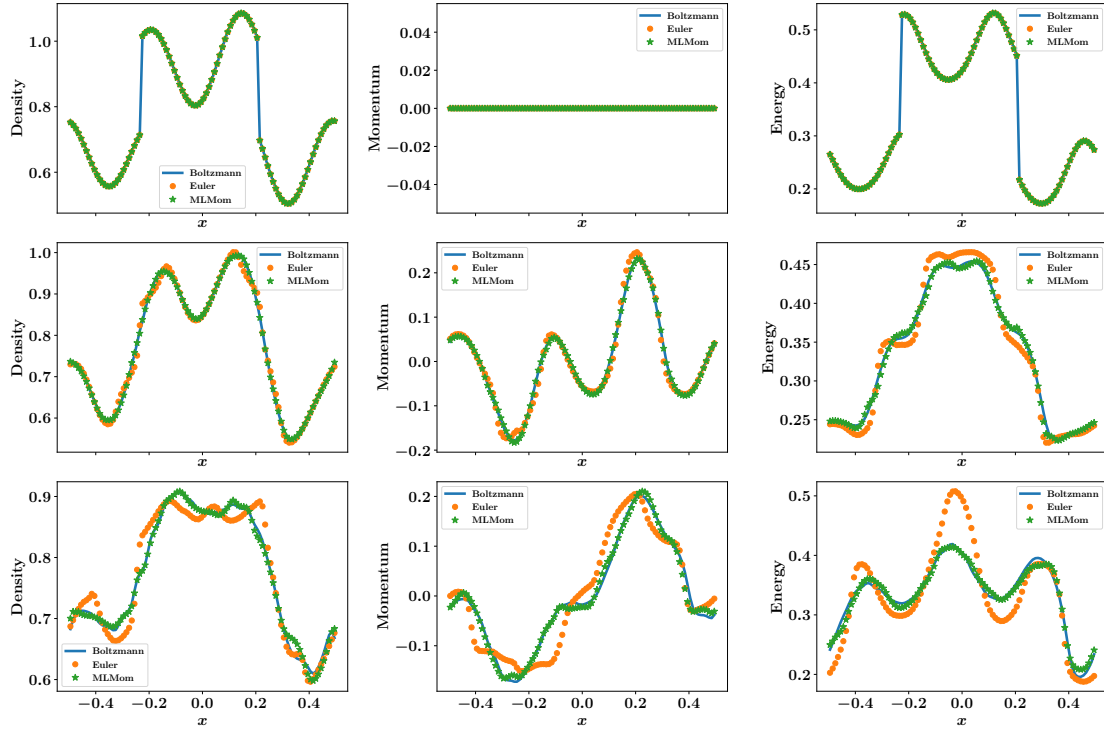


FIGURE 9. Sample profiles of density, momentum, and energy (from left to right) at  $t = 0, 0.05, 0.1$  (from top to bottom) in *Task MixIn-Transition*, obtained from the kinetic equation, the Euler equations, and MLMom.